A Nanoelectronic Enzyme-Linked Immunosorbent Assay for Detection of Proteins in Physiological Solutions

Eric Stern, Aleksandar Vacic, Chao Li, Fumiaki N. Ishikawa, Chongwu Zhou, Mark A. Reed, and Tarek M. Fahmy**

Semiconducting nanowires are promising ultrasensitive, label-free sensors for small molecules, DNA, proteins, and cellular function. Nanowire field-effect transistors (FETs) function by sensing the charge of a bound molecule. However, solutions of physiological ionic strength compromise the detection of specific binding events due to ionic (Debye) screening. A general solution to this limitation with the development of a hybrid nanoelectronic enzyme-linked immunosorbent assay (ne-ELISA) that combines the power of enzymatic conversion of a bound substrate with electronic detection is demonstrated. This novel configuration produces a local enzyme-mediated pH change proportional to the bound ligand concentration. It is shown that nanowire FETs configured as pH sensors can be used for the quantitative detection of interleukin-2 in physiologically buffered solution at concentrations as low as 1.6 pg mL^{-1}. By successfully bypassing the Debye screening inherent in physiological fluids, the ne-ELISA promises wide applicability for ligand detection in a range of relevant solutions.

Keywords:
- ELISA
- field-effect transistors
- nanowires
- sensors

1. Introduction

Single-crystal, semiconducting nanowire field-effect transistor (FET) devices[1–6] are attractive biosensors due to their extreme sensitivity to bound charges and potential portable format.[7–10] Nanowire devices configured as solution-phase sensors or ion-sensitive FETs (ISFETs) have been demonstrated as ultrasensitive sensors for small molecules,[11–15] DNA,[16–20] proteins,[11,12,19,21–27] and cellular function.[12,28] However, solutions with physiological salt concentrations have ionic (Debye) screening lengths of ≈0.7 nm, effectively neutralizing the molecular charge of the bound ligand beyond this distance. Thus, detection of such surface-bound ligands requires measurements to be performed in a low-salt (1.5 mM) buffer to increase the Debye screening length.[19]

To overcome this limitation, we devised a method that effects a pH change in a solution upon specific ligand binding. Our approach is similar to an enzyme-linked immunosorbent assay (ELISA),[29] but correlates protein presence with an enzyme-induced pH increase rather than the traditional colorimetric change (Figure 1A). Because of this similarity, we term our assay a nanoelectronic ELISA, or ne-ELISA. In our previous work, we used unfunctionalized nanowires as sensors to detect changes in the local pH microenvironment resulting from stimulation-induced alterations in cellular metabolism,[12,28] and Wang et al. recently used nanowire-based pH monitors to determine glucose concentrations, demonstrating the utility of nanowire sensors for indirect

[*] Prof. M. A. Reed, Prof. T. M. Fahmy, A. Vacic,[†] Dr. E. Stern[†§]
Departments of Electrical, Biomedical, and Chemical Engineering and Applied Physics
School of Engineering, Yale University
15 Prospect St, New Haven, CT 06511 (USA)
E-mail: mark.reed@yale.edu; tarek.fahmy@yale.edu
Prof. C. Zhou, C. Li, F. N. Ishikawa
Department of Electrical Engineering
University of Southern California
3737 Watts Way, Los Angeles, CA 90089 (USA)
[†] These authors contributed equally to this work.
[§] Present address: Nanoterra, Cambridge, MA 02139 (USA)

Supporting Information is available on the WWW under the http://www.small-journal.com or from the authors.

DOI: 10.1002/smll.200901551

NANO MICRO small

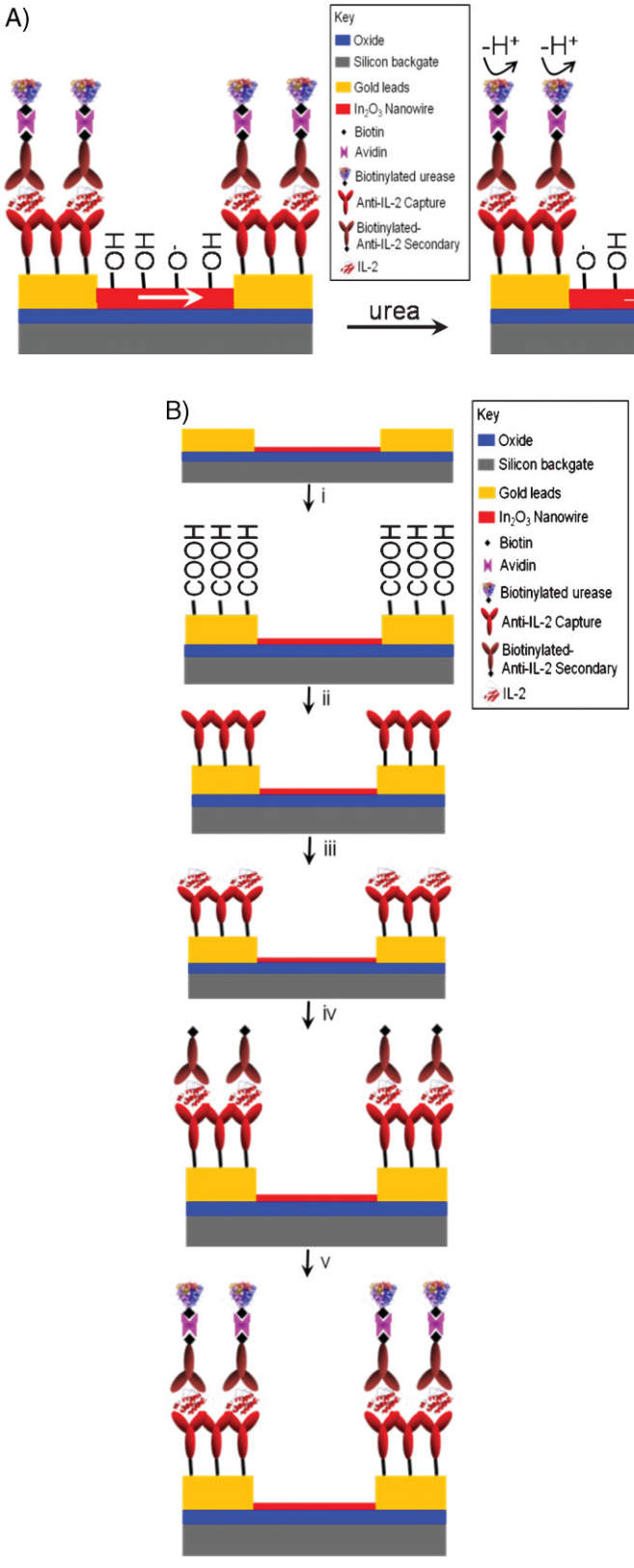

Figure 1. A) Schematic image of the ne-ELISA approach. Before the addition of urea the indium oxide surface is relatively protonated, inducing a relatively large channel current (large white arrow). The addition of urea results in the removal of protons from the solution and, thus, increased deprotonation of the nanowire surface. This, in turn, induces a decrease in the channel current (small white arrow). B) Surface functionalization schematic. The steps are described in the text and detailed in the Experimental Section.

molecular detection.[15] Increasing pH deprotonates surface hydroxyl groups on the nanosensors, resulting in a net decrease in positive gate charge and, in turn, a decrease in channel current for n-type devices.[30] By monitoring the urease-induced pH increase, we calculate the quantity of bound protein in a configuration that eliminates concerns over Debye screening in high-salt buffers[18,19] and nanowire-specific functionalization schemes[12,18] in a format that can be adapted for use in a variety of settings from the bench to the clinic.

2. Results and Discussion

Indium oxide nanowires were chosen because of their previously demonstrated utility as sensors.[23–25] As reported previously, these nanowires were grown by the laser-ablated hot-wall chemical vapor deposition method using a gold catalyst.[31] Devices were fabricated on 2-inch wafers with a global backgate, and contacts to the nanowires were defined with a nickel/gold (Ni/Au) stack, as detailed in earlier reports.[2] After preliminary screening, the wafers were diced and functionalized, as shown in Figure 1B.[32,33] This scheme solely functionalizes the gold leads,[32,33] and thus the surface hydroxyl groups on the indium oxide nanowires are maintained and are available for protonation and deprotonation,[34,35] which is necessary for measuring the solution pH. Figure 2 shows a scanning electron micrograph of a representative device, a ≈50-nm-diameter nanowire between Ni/Au leads.

Samples were first treated with ω-mercaptocarboxylic acid (Figure 1B i) to confer carboxylic acid functionality to the gold leads through thiol-mediated self-assembled monolayer (SAM) formation, as shown previously.[32,33] In this work, gold leads contacting the nanowires were used for convenience; however, any exposed gold surface in proximity to the sensor could be utilized. The gold surface is passivated by SAM formation, which can be demonstrated using cyclic voltametery.[36] In Figure 3, the redox peaks due to the exposed gold surface are significantly reduced after functionalization, indicating the formation of a functional surface.[36]

SAM formation on the gold leads minimally affects the electrical properties of the indium oxide nanowires. This is shown in the pre- and postfunctionalization dependence

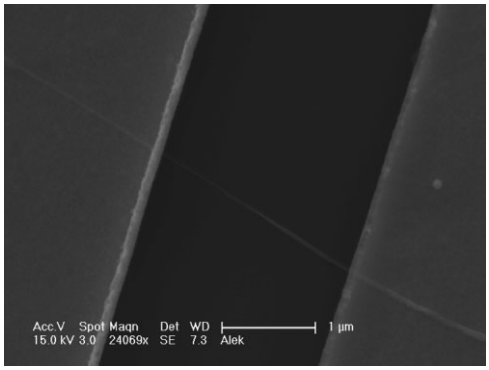

Figure 2. Scanning electron microscopy (SEM) image of a representative In_2O_3 nanowire FET sensor contacted by two parallel Ni/Au leads.

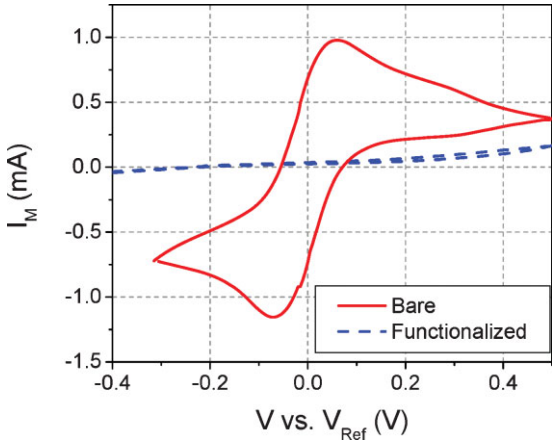

Figure 3. Cyclic voltammogram for an unfunctionalized (bare) and HS-$(CH_2)_n$-COOH-functionalized device demonstrating passivation of the Au leads. The solution is 50 mM Fe^{2+}/Fe^{3+} in 0.1 M KCl. Five sweeps were performed at 100 mV s^{-1} and the fifth of these is shown for each device.

of the drain–source current on drain–source voltage, $I_{DS}(V_{DS})$, for varying gate–drain voltage, V_{GD}, in Figure 4. The insets show the $I_{DS}(V_{GD})$ dependence for the $V_{DS} = 0.5$V operating point used in all sensing experiments. The postfunctionalization characteristics show that SAM formation does decrease the threshold voltage (V_t, thus increasing I_{DS} for a set V_{GD} in postfunctionalized devices),[30] but has a minimal effect on the transconductance at the operating point used for sensing ($V_{GD} = 0$V). Additionally, the subthreshold leakage current is also slightly increased, but to a level 100-fold lower than that used for sensing.

We first characterized the pH sensitivity of the In_2O_3 nanowires. Conventional indium tin oxide ISFETs have been previously demonstrated to have a linear pH sensitivity between pH 2 and 12,[34,35] thus we expected undoped In_2O_3 to exhibit a similar response. The response of a characteristic device to changes in pH, achieved by completely exchanging the sensing reservoir with buffers of different pH (pH = 8.0 initially, and pH = 9.0 and 10.0, at times $t = 0$ s and $t = 57.25$ s, respectively) is shown in Figure 5. The operating point for this device is $V_{DS} = 0.5$ V and $V_{GD} = 0$ V. The I_{DS} of the n-type In_2O_3 nanowires decreases with increasing pH due to the decreasing degree of protonation of the surface hydroxyl groups. Fluid injection induces transients that settle to a steady state within 20 s. Devices respond linearly to unit steps in pH in the pH 8–10 range.

To accurately calibrate the device's pH response, we measured the transconductance (g_m) while devices were immersed in solution. This is termed the solution transconductance. To create a reservoir for fluid handling, a poly(dimethylsiloxane) (PDMS) gasket[37] capable of holding ≈4 μL was placed over the die (see Supporting Information, Figure S1). Gating of the device was achieved through the solution by submerging the gate and reference electrodes into the buffer (the drain and reference electrodes were connected). Figure 6 shows the effect of solution gating a representative device. The device-to-solution leakage current ($I_{LEAKAGE}$, Figure 6) remains two orders of magnitude below the device current (I_{DS}) for $V_{GD} < 0.8$ V. Thus, to calculate the solution g_m, a linear best fit is made to the solution-phase I_{DS}-versus-V_{GD} plot for $0 \le V_{GD} \le 0.8$ V. The device sensitivity shows a clear correlation between increasing pH and solution g_m, demonstrated in Figure 7 for four different devices. A linear fit to this data yields a trendline that is within 6.7% error of the value of each I_{DS}/ΔpH datapoint. The device sensitivity can be calculated by dividing ΔI per pH unit by the solution g_m. The average sensitivity of the four devices shown in Figure 7 is 18.2 ± 1.2 mV per pH unit, a value below the maximum sensitivity of an ISFET, which is the ideal Nernst potential of 58 mV per pH unit.[13,38]

To demonstrate the capability of the ne-ELISA for the detection of labile macromolecules, we focused on the cytokine interleukin-2 (IL-2), whose presence reports on the activity of the T-cell immune response.[39] In the initial step, a capture IL-2 monoclonal antibody was conjugated to the carboxylic groups on the gold leads through its *N*-terminus (Figure 1B ii).[40] This was followed by a washing step that removed unbound capture antibodies (all binding steps described below are followed by washes) and the subsequent placement of a PDMS gasket over the nanowire devices to create the sensing reservoir.

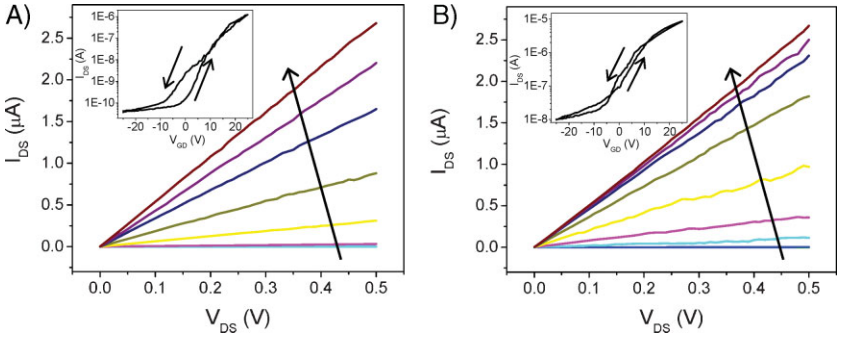

Figure 4. A) Unfunctionalized and B) functionalized ω-mercaptocarboxylic acid $I_{DS}(V_{DS})$ characteristics for V_{GD} increased from −25 V to 25 V in 5 V increments for a single representative device. The arrow shows increasing V_{GD}. The insets show the $I_{DS}(V_{GD})$ characteristics for $V_{DS} = 0.5$ V for the same device and the arrows indicate the sweep direction. The operating point for sensing measurements was $V_{DS} = 0.5$ V and $V_{GD} = 0$V.

NANO MICRO small

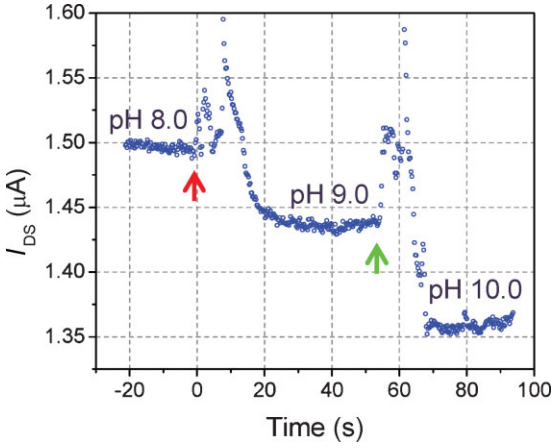

Figure 5. Device response to unit changes in pH. For $t < 0$, a pH 8.0 buffer was present in the reservoir. At $t = 0$ (red arrow) this buffer was exchanged with a buffer at pH 9.0, and at $t = 57.25$ s (green arrow) a second exchange, with a pH 10.0 buffer, was performed. All buffers were 0.01X PBS with 150 mM NaCl and were titrated using NaOH and HCl.

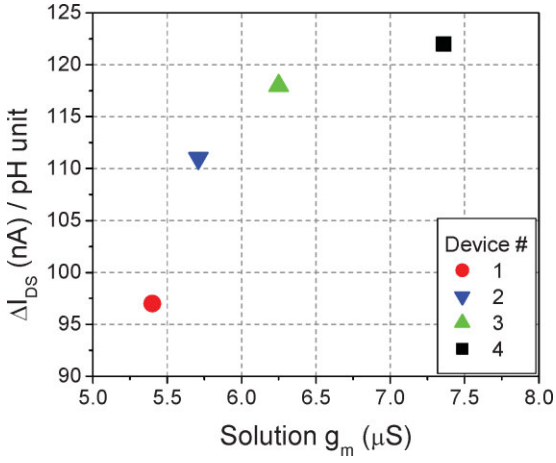

Figure 7. Scatter plot of the ΔI_{DS}-per-pH-unit response versus the solution transconductance (g_m) values for four In_2O_3 nanowire devices, as indicated in the legend. The R^2 value of the linear fit described in the text is 0.75.

Next, a bovine serum albumin (BSA) solution was used to prevent nonspecific protein adsorption to the chip and reservoir sidewalls, which is a typical blocking step used in conventional colorimetric ELISA protocols to minimize nonspecific binding.[29,41] This was followed by the addition of IL-2 at varying concentrations (across different devices) to the reservoir (Figure 1B iii). A secondary, biotinylated antibody to IL-2 was then introduced (Figure 1B iv), followed by the addition of neutravidin, a tetravalent biotin-binding protein,[41] and biotinylated urease (Figure 1B v).

The principle of the ne-ELISA is illustrated schematically in Figure 1B. Urease (here, bound via neutravidin–biotin to the secondary antibody) hydrolyzes free urea in the nanosensor reservoir according to the following reaction:[42,43]

$$Urea + 2H_2O + H^+ \xrightarrow{urease} 2NH_4^+ + HCO_3^- \quad (1)$$

Thus, the introduction of urea to the reservoir raises the solution pH, thereby decreasing I_{DS}.[42,44] Urea is added at a sufficient concentration for the urease to catalyze Equation 1 ($\approx 10^5$:1 molar ratio of urea to urease) at its maximum velocity,[40,45] and thus the rate of change in I_{DS} will correlate directly with the quantity of bound urease and, in turn, bound IL-2.

The operation of the ne-ELISA is demonstrated in Figure 8. The reservoir was half filled (2 μL) with the sensing buffer (0.01X phosphate buffered saline (PBS) plus 150 mM sodium chloride) at an initial pH = 8.0.[12,19,45] The devices were stabilized for 5–10 min under active measurement conditions ($V_{DS} = 0.5$V, $V_{GD} = 0$V). This equilibration time was required for the channel current (I_{DS}) to reach a steady state and is similar to that required for the elimination of initial background current in conventional ISFET glucose sensors.[46,47] During the sensing measurements, 2 μL of a 100 μM urea solution in the

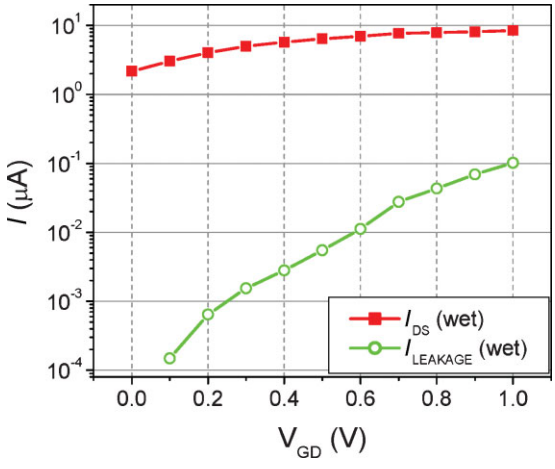

Figure 6. I_{DS}-versus-V_{GD} dependencies for a solution-gated (red) device. Solution gating was performed in the pH 8.0 buffer described in the text. The green data plot shows the leakage current of the device ($I_{LEAKAGE}$) during the solution-gating measurement.

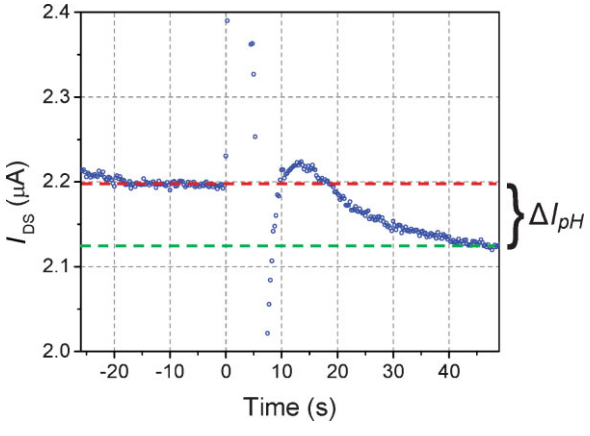

Figure 8. Response ($I_{DS}(t)$) of the sensor configured for IL-2 detection with 25 pg mL^{-1} IL-2 present during the protein-binding step (Figure 1B iii). At $t = 0$, the 100 μM urea solution was added to the pH 8.0 buffer. For this device, $\Delta I_{pH} = 68.0$ nA. The dashed red and green lines show the initial and final I_{DS} levels, respectively.

same pH 8.0 buffer was manually added with a micropipette, and the solution was mixed by micropipette mixing for ≈5–10 s. Introduction of this solution occurred at $t = 0$ in all figures. The response of a device to the presence of 12.5 pg mL^{-1} solution of IL-2 is shown in Figure 8. The decrease in I_{DS} and its continued negative derivative indicated that the addition of the urea solution resulted in a continuous drop in pH throughout the course of the measurement. The decrease in slope over time (similar to a conventional ELISA) is most likely due to a product of both the slowing of enzyme activity with increasing pH, [48] and the pH-dependant deviation (decrease) from ideal Nernstian behavior of an oxide surface.[49]

The key detection parameter is the asymptotic current difference (ΔI_{pH}), calculated by subtracting I_{DS} ($t \geq 40$ s) from I_{DS} ($t < 0$ s). Thus, the transient current spikes observed during urea addition and subsequent mixing do not interfere with the assay. For the device shown in Figure 8, $\Delta I_{pH} = 68.0$ nA. To demonstrate that this decrease in I_{DS} was due to urease activity, and not due to the addition of the urea solution, a control device without bound urease was used. Upon introduction of the urea solution, a decrease in I_{DS} of 1.8 nA was observed ($\Delta I_{pH} =$ 1.8 nA; see Supporting Information, Figure S2), setting this value as the assay's lower sensitivity limit.

The detection sensitivity of the ne-ELISA was determined by treating devices with decreasing concentrations of IL-2. We measured device responses to six serial dilutions of IL-2, starting with a concentration of 100 pg mL^{-1}. The device response to the median concentration, 12.5 pg mL^{-1}, is shown in Figure 8. The responses of the seven devices were converted into ΔpH changes by fitting the solution transconductance values of the devices (determined as described above after sensing measurements were completed) to the trendline determined from the control devices in Figure 7. Due to the nature of the assay (Figure 1), each device could be used only once, thus each datapoint is derived from a single device. Reproducibility of device response is not a concern since each device is individually calibrated prior to sensor use. The ΔpH versus IL-2 concentration is plotted in Figure 9, and

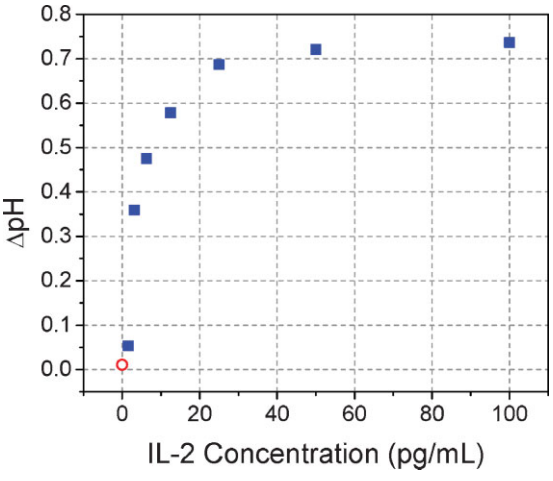

Figure 9. Plot of the ΔpH value measured by eight devices against the IL-2 concentration incubated with each sensor. The red circle derives from a control device to which no IL-2 was added during the protein-binding step (Figure 1B iii).

demonstrates the sensitivity of the assay as low as <1.6 pg mL^{-1} and in the range of IL-2 concentrations relevant for T-cell stimulation.[50,51] We note that the ΔpH-versus-IL-2-concentration calibration curve is nonlinear, primarily because pH is a logarithmic scale (–log[H$^+$]) versus linear analyte concentration (and to a lesser degree, the decrease in activity and response with increasing pH).

Although the minimum sensitivity shown here, <1.6 pg mL^{-1}, is only a factor of 2–4 better than conventional IL-2 ELISAs (USCN-LIFE, RayBio, and eBioscience kits), the power of this approach lies in the number of enzymes required to observe a signal. The results from the 1.6 pg mL^{-1} IL-2 sample were obtained from ≈8.4×10^4 urease molecules (see Supporting Information), compared with the ≈5.7×10^9 horseradish peroxidase molecules required to observe a colorimetric response in a conventional ELISA (Figure S3). This four-orders-of-magnitude improvement is due to the significantly greater sensitivity with which pH can be measured with nanowires compared to that with which absorbance can be measured optically.

3. Conclusions

Using nanowires, we have demonstrated a novel method for quantitative protein sensing in solutions with physiological salt concentrations. This new application utilizes enzymatic activity to overcome the critical Debye screening limitation associated with nanowire-FET sensing.[12,18,19,52] Given the generality of this approach for protein sensing, sensitivity can be practically tuned by adjustment of the surface area available for protein binding, or by choice of enzymes catalyzing solution ionic changes. Thus, the utility of this method is broad and durable, since it depends on the interplay between physical scaling of the devices and biochemical properties of the enzymes, in contrast with direct nanowire sensing, where sensitivity is solely dependent on nanowire dimensions. Variations of this technology with different device architectures or enzyme choices could potentially produce even more sensitive indirect nanowire sensors with fast response times operating in buffers with physiological salt concentrations, which can be of benefit in a wide variety of applications in biology and medicine.

4. Experimental Section

PDMS gasket fabrication: The silicone elastomer base and curing agent from the PDMS kit (Dow Corning) were mixed in a weigh boat in a 10:1 (w/w) ratio. The boat was then placed in a desiccator to remove air bubbles (≈10 min). The solution was poured onto a microscope slide to a level of ≈5 mm above the glass slide and was subsequently baked for two hours at 65 °C to harden the PDMS.[37] A metal tube with a 1.5-mm outer diameter (Small Parts, Inc.) and a sharpened end was used to punch holes in the PDMS, and a razor blade was used to free the gaskets from the PDMS sheets. These gaskets were pressed onto dies to create the sensor wells (Figure S1).

NANO MICRO small

Device fabrication: The In_2O_3 nanowires used for this study were synthesized on a Si/SiO_2 substrate (Silicon Quest International) by the previously described laser-ablation-assisted chemical vapor deposition method.[31] In order to transfer the nanowires from this growth substrate to the 2-inch Si/SiO_2 wafers (degenerately doped; 200-nm oxide; Silicon Quest International) used for device processing, the nanowires were suspended in semiconductor-processing-grade isopropanol (Brand Nu Labs) by ultrasonic agitation (10–20 sec). Optical lithography was then used to create leads that contacted the randomly dispersed nanowires, as detailed in earlier reports.[2,53] Briefly, a photoresist bilayer was applied (LOR10A/S1808; MicroChem, Inc.), patterned, and subjected to an oxygen plasma. Wafers were then loaded into an electron-beam (e-beam) evaporator (Denton Vacuum Systems) and deposited with a 50-nm Ni (99.9%, Kurt J. Lesker Co.)/200-nm Au (99.5%, Kurt J. Lesker Co.) stack. Lift off was then performed with *N*-methyl pyrrolidone (VWR Scientific). Note that the wafers were patterned with topside contacts to the degenerate Si prior to nanowire dispersion.

The wafers were screened for functional nanowire FETs by measuring the dependence of the source–drain current (I_{DS}) on the source–drain voltage (V_{DS}) with varying gate–source voltage (V_{GS}). A Cascade Microtech automated probe station interfaced with a HP4156B semiconductor parameter analyzer controlled by in-house-written Lab View and Mathematica codes was used for screening. Leakage currents were <10 pA, well below device I_{DS} levels.

Device preparation for cyclic voltammetry measurements: The gold-coated substrates used in cyclic voltammetry (CV) experiments were prepared by an e-beam evaporation of a 5-nm Cr (99.9%, Kurt J. Lesker Co.)/70-nm Au (99.99% Cerac, Inc.) stack onto Si wafers (Silicon Quest International) previously cleaned with piranha (1:3 H_2O_2:H_2SO_4; J.T. Baker Co.), acetone (Sigma), methanol (Sigma), and deionized water and then blown dry with nitrogen. The substrates were then immersed in a solution of ω-mercaptocarboxylic acid (1 mM) prepared in deoxygenated, absolute ethanol and left for 12 h in the dark in an inert atmosphere.[32] The samples were subsequently washed with ethanol, toluene (Sigma), and isopropanol (Sigma) and blown dry with a directed stream of nitrogen. The CV measurements were performed using a Gamry Femtostat using a Pt counter electrode (Ernest F. Fullham, Inc.) and an Ag/AgCl reference electrode fabricated by the electrodeposition of AgCl on an Ag wire (Ernest F. Fullham, Inc.) from a saturated aqueous solution of NaCl (Sigma).

Biotin–urease conjugation: (+)-biotinamidohexanoic acid hydrazide (biotin-LC-hydrazide; 3 mg; Pierce Scientific) was dissolved in dimethyl sulfoxide (DMSO) (500 μL, Sigma) and added to a solution of jack bean urease (1 mg mL^{-1}; Sigma, Cat. No. 94285) and 1-ethyl-3-[3-dimethylaminopropyl]carbodiimide hydrochloride (EDC; 5 mg mL^{-1}; Pierce Scientific) in PBS (3mL; Sigma).[41] The reaction proceeded for 1 h at room temperature with shaking. After the conjugation was complete, the product was isolated by centrifugation using a 50-mL Amicon Ultra (Millipore, Cat. No. UFC905024) centrifugal filter tube with a 50 000 MW cutoff (four 30-min spins at 3000 rpm at 4 °C). The resulting biotin–urease was diluted to 0.1 mg mL^{-1} and stored at 4 °C.

Device functionalization: Dies containing working devices were diced from the wafer and were functionalized with ω-mercaptocarboxylic acid as described above. The functionalized devices were first treated with a solution of the capture anti-IL-2 antibody (0.1 mg mL^{-1}; BD Biosciences, Cat. No. 555051) in PBS with EDC (0.05 mg) and *N*-hydroxysulfosuccinimide (sulfo-NHS; 0.025 mg; Pierce Scientific) for 1 h.[41] Washing was performed three times using PBS, followed by the addition of a BSA (10%; Sigma) solution, after which washing was again performed. Next, IL-2 (Novartis) was added at varying concentrations, as described in the text, for 1 h. Periodic pipetting, up and down, was performed to maximize protein binding. After washing three times with PBS, a solution of avidin-conjugated anti-IL-2 detection antibody (0.1 mg mL^{-1}) was added for 1 h. This conjugate was generated by adding equal molar amounts of streptavidin (Pierce Scientific) and biotinylated anti-IL-2 (BD Biosciences, Cat. No. 555040) and allowing the binding to occur for 15 min at room temperature in PBS. The conjugates were stored at 4 °C and used without further purification. After washing three times with PBS, a solution of biotin–urease (0.1 mg mL^{-1}) in PBS was added for 1 h. Washing was again performed three times with PBS, and devices were then washed and stored in the sensing buffer (0.01X PBS+150 mM NaCl, pH 8.0) directly prior to use. The sensing buffer was titrated to pH 8.0 with solutions of HCl (1N, J.T. Baker) and NaOH (1N, J.T. Baker).

Sensing measurements: First, a baseline current level was established with a 2-μL sensing buffer (see above) in the reservoir. A HP4156B was used for all sensing measurements. The PBS was diluted 100 fold to decrease its buffering capability; otherwise, the urease-catalyzed decrease in the $[H^+]$ would be buffered (no pH change would result). Device stabilization under active measurement conditions ($V_{DS} = 0.5$V; $V_{GD} = 0$V) required 10–20 min. After device stabilization, sensing experiments could be performed. The drain–source current was monitored versus time (active measurement conditions were $V_{DS} = 0.5$V, $V_{GD} = 0$V). After ≈60 s to establish a steady baseline current, 2 μL of a 100 μM solution of urea (Sigma) in sensing buffer was added (at $t = 0$). The temporal response of sensor channel current (I_{DS}) to the addition of the 100 mM urea sensing solution to the pH 8.0 buffer in the absence of bound urease is shown in Figure S2. The average ΔI_{pH} for the control devices was 2.5 nA (ΔI_{pH} for the device shown in Figure S2 is 3.1 nA). After the sensing measurements, the devices were solution gated to determine the solution transconductance, which is required for sensitivity calculations.

Acknowledgements

This paper is dedicated in loving memory to Alan Stern. The authors thank J. Criscione and D. Routenberg for helpful discussions, and K. Milnamow for critical reading of the manuscript. This work was partially supported by ARO, NIH RO1 (EB008260), and by CIfAR.

[1] W. Lu, C. M. Lieber, *Nat. Mater.* **2007**, *6*, 841–850.
[2] E. Stern, G. Cheng, J. F. Klemic, E. Broomfield, D. Turner-Evans, C. Li, C. Zhou, M. A. Reed, *J. Vac. Sci. Technol. B* **2005**, *24*, 231–236.

[3] Y. Huang, X. Duan, Q. Wei, C. M. Lieber, *Science* **2001**, *291*, 630–633.
[4] J.-H. Ahn, H.-S. Kim, K. J. Lee, S. Jeon, S. J. Kang, Y. Sun, R. G. Nuzzo, J. A. Rogers, *Science* **2006**, *314*, 1754–1757.
[5] O. Englander, D. Christensen, J. Kim, L. Lin, S. J. S. Morris, *Nano Lett.* **2005**, *5*, 705–708.
[6] J. Goldberger, A. I. Hochbaum, R. Fan, P. Yang, *Nano Lett.* **2006**, *6*, 973–977.
[7] F. Patolsky, C. M. Lieber, *Mater. Today* **2005**, *4*, 20–28.
[8] F. Patolsky, G. Zheng, C. M. Lieber, *Anal. Chem.* **2006**, *78*, 4260–4269.
[9] E. T. Carlen, A. van den Berg, *Lab Chip* **2007**, *7*, 19–23.
[10] D. Grieshaber, R. MacKenzie, J. Voros, E. Reimhult, *Sensors* **2008**, *8*, 1400–1458.
[11] Y. Cui, Q. Wei, H. Park, C. M. Lieber, *Science* **2001**, *293*, 1289–1292.
[12] E. Stern, J. F. Klemic, D. A. Routenberg, P. N. Wyrembak, D. B. Turner-Evans, A. D. Hamilton, D. A. LaVan, T. M. Fahmy, M. A. Reed, *Nature* **2007**, *445*, 519–522.
[13] Y. Chen, X. Wang, S. Erramilli, P. Mohanty, A. Kalinowski, *Appl. Phys. Lett.* **2006**, *89*, 223512.
[14] X. Bi, W. L. Wong, W. Ji, A. Agarwal, N. Balasubramanian, K.-L. Yang, *Biosens. Bioelectron.* **2008**, *23*, 1442–1448.
[15] X. Wang, Y. Chen, K. A. Gibney, S. Erramilli, P. Mohanty, *Appl. Phys. Lett.* **2008**, *92*, 013903.
[16] J.-i. Hahm, C. M. Lieber, *Nano Lett.* **2004**, *4*, 51–54.
[17] Z. Li, Y. Chen, X. Li, T. I. Kamins, K. Nauka, R. S. Williams, *Nano Lett.* **2004**, *4*, 245–247.
[18] Y. L. Bunimovich, Y. S. Shin, W.-S. Yeo, M. Amori, G. Kwong, J. R. Heath, *J. Am. Chem. Soc.* **2006**, *128*, 16323–16331.
[19] E. Stern, R. Wagner, F. J. Sigworth, R. Breaker, T. M. Fahmy, M. A. Reed, *Nano Lett.* **2007**, *7*, 3405–3409.
[20] G.-J. Zhang, G. Zhang, J. H. Chua, R.-E. Chee, E. H. Wong, A. Agarwal, K. D. Buddharaju, N. Singh, Z. Gao, N. Balasubramanian, *Nano Lett.* **2008**, *8*, 1066–1070.
[21] W. U. Wang, C. Chen, K.-h. Lin, Y. Fang, C. M. Lieber, *Proc. Natl. Acad. Sci. USA* **2005**, *102*, 3208–3212.
[22] G. Zheng, F. Patolsky, Y. Cui, W. U. Wang, C. M. Lieber, *Nat. Biotechnol.* **2005**, *23*, 1294–1301.
[23] C. Li, M. Curreli, H. Lin, B. Lei, F. N. Ishikawa, R. Datar, R. J. Cote, M. E. Thompson, C. Zhou, *J. Am. Chem. Soc.* **2005**, *127*, 12484–12485.
[24] M. Rouhanizadeh, T. Tang, C. Li, J. Hwang, C. Zhou, T. K. Hsiai, *Sens. Actuators B* **2006**, *114*, 788–798.
[25] T. Tang, X. Liu, C. Li, B. Lei, D. Zhang, M. Rouhanizadeh, T. K. Hsiai, C. Zhou, *Appl. Phys. Lett.* **2005**, *86*, 103903.
[26] A. Kim, C. S. Ah, H. Y. Yu, J.-H. Yang, I.-B. Baek, C.-G. Ahn, C. W. Park, M. S. Jun, *Appl. Phys. Lett.* **2007**, *91*, 103901.
[27] N. Elfstrom, A. E. Karlstrom, J. Linnros, *Nano Lett.* **2008**, *8*, 945–949.
[28] E. Stern, E. R. Steenblock, M. A. Reed, T. M. Fahmy, *Nano Lett.* **2008**, *8*, 3310–3314.
[29] J. R. Crowther, *Elisa: Theory and Practice*, Humana Press, New York **1995**.
[30] S. M. Sze, *Physics of Semiconductor Devices*, 2nd ed. John Wiley & Sons, New York **1981**.
[31] C. Li, D. Zhang, S. Han, X. Liu, T. Tang, C. Zhou, *Adv. Mater.* **2003**, *15*, 143–146.
[32] C. D. Bain, G. M. Whitesides, *Langmuir* **1989**, *5*, 1370–1378.
[33] S. R. Wasserman, Y.-T. Tao, G. M. Whitesides, *Langmuir* **1989**, *5*, 1074–1087.
[34] L.-T. Yin, J.-C. Chou, W.-Y. Chung, T.-P. Sun, S.-K. Hsiung, *Sens. Actuators B* **2000**, *71*, 106–111.
[35] L.-T. Yin, J.-C. Chou, W.-Y. Chung, T.-P. Sun, S.-K. Hsiung, *Mater. Chem. Phys.* **2001**, *70*, 12–16.
[36] C. E. D. Chidsey, D. N. Loiacono, *Langmuir* **1989**, *6*, 682–691.
[37] D. C. Duffy, J. C. McDonald, O. J. A. Schueller, G. M. Whitesides, *Anal. Chem.* **1998**, *70*, 4974–4984.
[38] J. Israelachvili, *Intermolecular & Surface Forces*, 2nd ed. Academic Press, London **1991**.
[39] P. Jin, E. Wang, M. Provenzano, D. Stroncek, F. M. Marincola, *Crit. Rev. Immunol.* **2007**, *27*, 437–448.
[40] D. J. Voet, J. G. Voet, *Biochemistry*, 3rd ed. John Wiley & Sons, New York **2005**.
[41] G. T. Hermanson, *Bioconjugate Techniques*, Elsevier Science & Technology Books, New York **1996**.
[42] A. P. Soldatkin, J. Montoriol, W. Sant, C. Martelet, N. Jaffrezic-Renault, *Biosens. Bioelectron.* **2003**, *19*, 131–135.
[43] A. G. Gehring, D. L. Patterson, S.-I. Tu, *Anal. Biochem.* **1998**, *258*, 293–298.
[44] I. Karube, T. Moriizumi, *Meth. Enzymol.* **1988**, *137*, 255–260.
[45] S. D. Cesareo, S. R. Langton, *FEMS Microbiol. Lett.* **1992**, *99*, 15–22.
[46] Y.-M. Uang, T.-C. Chou, *Electroanal.* **2001**, *14*, 1564–1570.
[47] D. Belanger, J. Nadreau, G. Fortier, *J. Electroanal. Chem.* **1989**, *274*, 143–155.
[48] B. Krajewska, S. Ciurli, *Plant Physiol. Biochem.* **2005**, *43*, 651–658.
[49] R. E. G. van Hal, J. C. T. Eijkel, P. Bergveld, *Adv. Colloid Interface Sci.* **1996**, *69*, 31–62.
[50] D. M. Pardoll, *Nat. Rev. Immunol.* **2002**, *2*, 227–238.
[51] K. S. Schluns, L. Lefrancois, *Nat. Rev. Immunol.* **2003**, *3*, 269–279.
[52] M. M.-C. Cheng, G. Cuda, Y. L. Bunimovich, M. Gaspari, J. R. Heath, H. D. Hill, C. A. Mirkin, A. J. Nijdam, R. Terracciano, T. Thundat, M. Ferrari, *Curr. Opin. Chem. Biol.* **2006**, *10*, 11–19.
[53] E. Stern, G. Cheng, E. Cimpoiasu, R. Klie, S. Guthrie, J. F. Klemic, I. Kretzschmar, E. Steinlauf, D. Turner-Evans, E. Broomfield, J. Hyland, R. Koudelka, T. Boone, M. P. Young, A. Sanders, R. Munden, T. Lee, D. A. Routenberg, M. A. Reed, *Nanotechnology* **2005**, *16*, 2941–2953.

Received: August 19, 2009
Published online: October 30, 2009

